

# Diversity-Preserved Distribution Matching Distillation for Fast Visual Synthesis

Tianhe Wu <sup>\*13</sup> Ruibin Li <sup>\*2</sup> Lei Zhang <sup>†23</sup> Kede Ma <sup>†1</sup>

<https://github.com/Multimedia-Analytics-Laboratory/dpdmd>



Figure 1. **DP-DMD preserves image diversity** while maintaining competitive visual quality. All results are generated under identical text conditioning (“A smiling woman with red hair, green eyes, and dimples.”) with different random initial noise. (a) SD3.5-M (Esser et al., 2024) sampled with 30 steps (60 NFEs) serves as the teacher model (upper bound). (b) DMD (Yin et al., 2024a) and (c) **DP-DMD** are step-distilled student models, both evaluated using only 4 NFEs.

## Abstract

Distribution matching distillation (DMD) aligns a multi-step generator with its few-step counterpart to enable high-quality generation under low inference cost. However, DMD tends to suffer from *mode collapse*, as its reverse-KL formulation inherently encourages mode-seeking behavior, for which existing remedies typically rely on perceptual or adversarial regularization, thereby incurring substantial computational overhead and training instability. In this work, we propose a role-separated distillation framework that explicitly disentangles the roles of distilled steps: the first step is dedicated to preserving sample diversity via a *target*-prediction (*e.g.*,  $v$ -prediction) objective, while subsequent steps focus on quality re-

finement under the standard DMD loss, with gradients from the DMD objective blocked at the first step. We term this approach Diversity-Preserved DMD (**DP-DMD**), which, despite its simplicity—*no perceptual backbone, no discriminator, no auxiliary networks, and no additional ground-truth images*—preserves sample diversity while maintaining visual quality on par with state-of-the-art methods in extensive text-to-image experiments.

## 1. Introduction

Generative modeling seeks to synthesize high-fidelity image data by learning complex data distributions through stochastic or continuous-time processes. Among the most influential approaches, diffusion models (Song et al., 2020) and their flow-based counterparts (Lipman et al., 2022) have driven remarkable progress in image and video generation (Esser et al., 2024; Wan et al., 2025), benefiting from recent advances in large-scale foundation models (Rombach et al., 2022; Labs et al., 2025) and modern optimization techniques (Sutton et al., 1999). Despite their success, these

<sup>\*</sup>Equal contribution <sup>1</sup>City University of Hong Kong <sup>2</sup>The Hong Kong Polytechnic University <sup>3</sup>OPPO Research Institute. Correspondence to: Lei Zhang <cslzhang@comp.polyu.edu.hk>, Kede Ma <kede.ma@cityu.edu.hk>.

methods require numerically integrating multi-step differential equations to realize generative dynamics, resulting in long inference-time and high computational cost due to the large number of function evaluations (NFEs).

To mitigate inference latency, prior distillation methods mainly follow a trajectory-based direction (Liu et al., 2023b; Yan et al., 2024), approximating the teacher’s sampling trajectory using fewer inference steps. More recently, this paradigm has shifted from trajectory approximation toward directly aligning the output distributions of teacher and student models by minimizing statistical divergences (Sauer et al., 2024b; Yin et al., 2024b;a; Liu et al., 2025). Among these approaches, distribution matching distillation (DMD) (Yin et al., 2024b) stands out as a representative framework, achieving both fast inference and high-quality generation. Nevertheless, as illustrated in Figure 1, optimizing the student model with the DMD loss leads to a substantial reduction in sample diversity compared to its multi-step counterpart. This arises from the reverse-KL formulation of DMD, which inherently encourages mode-seeking and consequently causes *mode collapse*.

To alleviate this issue, current mainstream methods (Yin et al., 2024b;a; Chadebec et al., 2025; Lu et al., 2025) augment the DMD objective with perceptual and adversarial losses, leveraging additional samples synthesized by the teacher as an implicit regularizer to promote more comprehensive coverage of the teacher distribution by the student model. However, the incorporation of such modules introduces non-negligible computational overhead<sup>1</sup>, as well as instability in adversarial training.

Motivated by the observations (see Figure A in the Appendix) from multi-step experiential sampling—where early denoising steps primarily determine the global structural layout and later steps progressively refine fine-grained visual details—we propose a role-separated distillation framework termed Diversity-Preserved DMD (**DP-DMD**). Specifically, we assign distinct roles to different distilled steps. The first distilled step is supervised using a *target*-prediction objective (e.g.,  $v$ -prediction), which encourages the student model to preserve sample diversity during generation. For the remaining distilled steps, we adopt the standard DMD objective, allowing these steps to focus on refining visual fidelity and overall image quality. To maintain this role separation, we stop gradients from the DMD loss at the first step, preventing the reverse-KL objective from overriding the diversity-preserving supervision.

Our proposed **DP-DMD** is deliberately simple: *no perceptual backbone, no discriminator, no auxiliary networks, and*

<sup>1</sup>Widely adopted perceptual losses, such as LPIPS (Zhang et al., 2018) and DISTS (Ding et al., 2020), incur significant GPU memory consumption and computational cost, especially when applied to high-resolution imagery.

*no additional ground-truth images*. Everything happens in latent space, keeping the pipeline compact, stable, and memory-efficient. Yet this minimalism does not come at the expense of performance: across extensive text-to-image (T2I) experiments, **DP-DMD** preserves sample diversity while maintaining visual quality on par with state-of-the-art methods under few-step sampling. We believe this work takes a step forward in diffusion distillation and offers insights to the broader research community.

## 2. Related Work

This section surveys recent few-step diffusion distillation methods and highlights key optimization challenges, including performance degradation and reduced sample diversity.

**Trajectory-based Methods.** Trajectory-based distillation methods aim to train a few-step student model by explicitly aligning its denoising trajectory with that of a multi-step teacher model (Song et al., 2023; Liu et al., 2023c; Luo et al., 2023; Meng et al., 2023; Lu & Song, 2024; Li et al., 2025). By selecting anchor points along the teacher’s trajectory, Consistency Models (Song et al., 2023; Song & Dhariwal, 2023) and subsequent extensions (Wang et al., 2024; Lu & Song, 2024) significantly shorten the denoising trajectory, enabling high-quality generation with only a few inference steps instead of the conventional tens of iterations. More recently, MeanFlow (Geng et al., 2025) proposes matching the average velocity of the diffusion trajectory, enabling further acceleration with only a handful of inference steps. Despite their empirical success, trajectory-based methods often exhibit significant performance degradation when applied to large-scale pretrained image synthesis or video generation models (Zheng et al., 2025).

**Distribution-Matching Methods.** Distribution-matching methods aim to distill multi-step diffusion models into efficient few-step generators by aligning the student model’s output distribution with that of a pretrained diffusion model. One line of work adopts GAN-based formulations, introducing auxiliary discriminators or reusing the diffusion model as a feature extractor to construct adversarial objectives (Sauer et al., 2024b;a; Lin et al., 2024; Zhou et al., 2024a). Although these methods can produce sharp samples, the instability of adversarial training often hampers scalability and robustness in large-scale diffusion distillation.

Another line of work is inspired by distribution matching in 3D generation (Wang et al., 2023a; Poole et al., 2022), where optimization minimizes the discrepancy between rendered images and diffusion model outputs. DMD (Yin et al., 2024b) adapts this paradigm to diffusion distillation and enables effective few-step generation, with subsequent extensions further improving performance by incorporating auxiliary losses (Zheng et al., 2025; Liu et al., 2025; Yin

et al., 2024a; Zhou et al., 2024b). Despite strong empirical results, DMD-based methods are prone to model collapse under prolonged training, leading to reduced **sample diversity**. Prior solutions mitigate this issue by introducing regression or GAN losses (Yin et al., 2024b;a), but at the cost of significant computational and memory overhead. In contrast, our **DP-DMD** maintains high-quality distillation and sample diversity without additional training modules, offering a more efficient and practical solution.

### 3. Background: Flow Matching and DMD

#### 3.1. Flow Matching

Diffusion models can be equivalently formulated using an ordinary differential equation (ODE) framework (Chen et al., 2018; Song et al., 2020). Given data samples  $\mathbf{x} \sim p_{\text{data}}(\mathbf{x})$  and prior noise samples  $\epsilon \sim p_{\text{noise}}(\epsilon)$  (e.g.,  $\epsilon \sim \mathcal{N}(0, \mathbf{I})$ ), a flow path can be constructed via a linear interpolation between data and noise as  $\mathbf{z}_t = a_t \mathbf{x} + b_t \epsilon$ , where  $t \in [0, 1]$  and  $a_t, b_t$  are predefined noise schedules. A widely used choice is the linear schedule (Liu et al., 2023b; Esser et al., 2024), defined by  $a_t = 1 - t$  and  $b_t = t$ , which yields:

$$\mathbf{z}_t = (1 - t) \mathbf{x} + t \epsilon. \quad (1)$$

We see that  $\mathbf{z}_t \sim p_{\text{data}}$  at  $t = 0$  and transitions to  $p_{\text{noise}}$  at  $t = 1$ . The associated flow velocity is defined as the time derivative of  $\mathbf{z}_t$ , namely  $\mathbf{v}_t = \mathbf{z}'_t = a'_t \mathbf{x} + b'_t \epsilon$ . By differentiating Equation 1 w.r.t.  $t$ , we have  $\mathbf{v}_t = \epsilon - \mathbf{x}$ .

Flow-based methods (Lipman et al., 2022; Geng et al., 2025) seek to learn a neural velocity field  $\mathbf{v}_\theta(\mathbf{z}_t, t)$  parameterized by  $\theta$ , through minimization of the following objective:

$$\mathcal{L}_{\text{FM}} = \mathbb{E}_{t, \mathbf{x}, \epsilon} \left[ \left\| \mathbf{v}_\theta(\mathbf{z}_t, t) - (\epsilon - \mathbf{x}) \right\|^2 \right]. \quad (2)$$

At inference time, novel samples are generated by solving the ODE induced by the learned velocity field  $\mathbf{v}_\theta$ , namely  $\frac{d}{dt} \mathbf{z}_t = \mathbf{v}_\theta(\mathbf{z}_t, t)$ , starting from a noise sample  $\mathbf{z}_1 \sim p_{\text{noise}}$  and integrating backward in time from  $t = 1$  to  $t = 0$ , which yields the data sample  $\mathbf{x}_\theta = \mathbf{z}_1 + \int_1^0 \mathbf{v}_\theta(\mathbf{z}_t, t) dt$ .

#### 3.2. DMD Loss

DMD aims to align the sample distribution produced by a few-step student with that generated by a high-quality multi-step teacher. It minimizes the divergence between the two distributions, defined as  $\mathcal{L}_{\text{DMD}} \triangleq D_{\text{KL}}(p_{\text{fake}}(\mathbf{x}_\theta) \parallel p_{\text{real}}(\mathbf{x}_\theta))$ , where  $p_{\text{fake}}$  and  $p_{\text{real}}$  denote the distributions induced by the student and the teacher, respectively. Although this KL divergence is intractable to evaluate explicitly in high-dimensional spaces (Pool et al., 2023; Wang et al., 2023a), its gradient with respect to the student parameters  $\theta$  admits a convenient form. Denoting by  $\mathbf{x}_\theta$  a sample generated by the student, the gradient of  $\mathcal{L}_{\text{DMD}}$  can

be written as:

$$\nabla_\theta \mathcal{L}_{\text{DMD}} = \mathbb{E}_{\mathbf{x}_\theta} \left[ (s_{\text{fake}}(\mathbf{z}_t) - s_{\text{real}}(\mathbf{z}_t)) \nabla_\theta \mathbf{x}_\theta \right], \quad (3)$$

where  $\mathbf{z}_t$  is obtained by diffusing the student sample  $\mathbf{x}_\theta$  according to Equation 1, so that the student- and teacher-induced distributions exhibit overlapping support in the perturbed space (Yin et al., 2024b). The corresponding score functions,  $s_{\text{fake}} = \nabla_{\mathbf{z}_t} \log p_{\text{fake}}(\mathbf{z}_t)$  and  $s_{\text{real}} = \nabla_{\mathbf{z}_t} \log p_{\text{real}}(\mathbf{z}_t)$ , are defined as the gradients of the log-densities associated with the student and teacher distributions in this space, respectively. While the teacher score  $s_{\text{real}}$  is directly available from the pretrained multi-step diffusion model, the student score  $s_{\text{fake}}$  is intractable and is therefore approximated using an auxiliary fake model<sup>2</sup>. Following (Yin et al., 2024a), the fake model is updated for  $M$  steps using Equation 2 before updating each student, yielding an accurate estimate of  $s_{\text{fake}}$  for the DMD objective.

### 4. DP-DMD for Diffusion Distillation

This section analyzes the roles of early and late denoising steps and presents **DP-DMD**, a role-separated distillation framework, with the training pipeline shown in Figure 2.

#### 4.1. Roles of Early and Late Denoising Steps

Recent studies on diffusion and flow-based generative models have consistently observed that the denoising process exhibits a clear stage-wise behavior (Wang & Vastola, 2023; Liu et al., 2023a; He et al., 2025).

**Early-Step Diversity Preservation.** As illustrated in Figure A of the Appendix, early denoising steps primarily operate at high noise levels and are responsible for recovering the global structural layout of the sample, such as object presence, coarse geometry, and overall composition. Importantly, variations introduced at these early stages tend to persist throughout the subsequent denoising trajectory, making them a key determinant of **sample diversity**.

**Late-Step Quality Refinement.** In contrast, later denoising steps operate at lower noise levels and focus on refining fine-grained visual details, including textures, colors, and local appearance. These steps exert limited influence on global structure and thus contribute mainly to perceptual quality rather than diversity.

This intrinsic asymmetry between early and late denoising steps suggests that treating all distilled steps uniformly, as done in standard DMD (Yin et al., 2024b;a), may be ineffective for preserving diversity. Instead, explicitly assigning different training objectives to different stages of the distilled process provides a principled opportunity to balance

<sup>2</sup>The fake model is initialized in the same way as the teacher model, and both share an identical architecture.

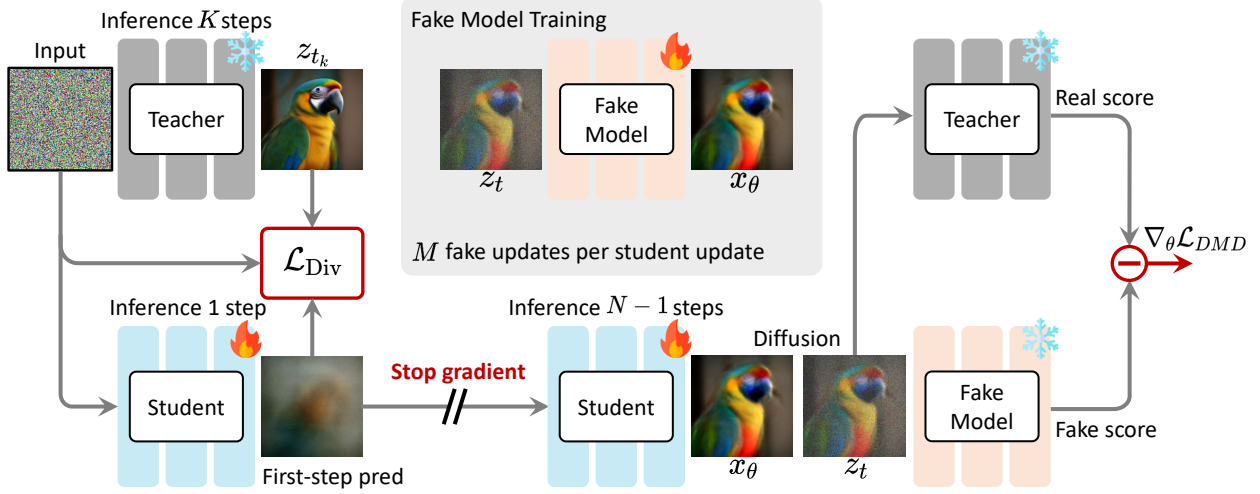


Figure 2. **Training pipeline of DP-DMD.** The first denoising step of the student is guided by a Flow-Matching diversity loss using a teacher-derived intermediate state, with gradients stopped thereafter. The remaining steps are optimized via the DMD objective, leveraging teacher and fake-model scores to refine sample quality. This role separation preserves diversity while maintaining high-fidelity generation in few-step distillation.

diversity preservation and quality refinement, which directly motivates our role-separated **DP-DMD** framework.

#### 4.2. Diversity-Preserved DMD

**Overview.** Given a distilled few-step student model with  $N$  inference steps, **DP-DMD** assigns different training objectives to different steps. Specifically, the *first* distilled step is supervised using a *target*-prediction objective (Equation 2) to encourage diversity preservation, while the remaining  $N - 1$  steps are optimized using the standard DMD loss (Equation 3) to refine visual quality. This separation enables the student to retain diverse global structures without sacrificing the efficiency and fidelity advantages of DMD.

**Diversity Supervision.** We begin by describing the construction of the supervision signal employed in the diversity-preserving stage. Given a multi-step teacher model, we carry out inference for a predefined number of steps  $K$ . Hyperparameter  $K$  controls the noise level, with which diversity is anchored. We denote by  $z_{t_k}$  the intermediate sample produced by the teacher at the  $k$ -th inference step, which corresponds to time  $t_k$  in the continuous flow formulation.

Following the linear flow path defined in Equation 1, the velocity target at time  $t_k$  is given by:

$$v_k^{\text{target}} = \frac{\epsilon - z_{t_k}}{1 - t_k}. \quad (4)$$

This target corresponds to the ground-truth flow velocity used to define the first-step transport from noise toward the teacher-produced intermediate state  $z_{t_k}$  under the linear interpolation assumption.

In the distilled model, the first step predicts a velocity field  $v_\theta(\epsilon, 1)$ , which is trained using a Flow Matching loss against the target defined in Equation 4:

$$\mathcal{L}_{\text{Div}} = \mathbb{E}_\epsilon \left[ \|v_\theta(\epsilon, 1) - v_k^{\text{target}}\|^2 \right]. \quad (5)$$

By explicitly aligning the student’s first-step prediction with a teacher-derived intermediate state, this objective encourages the student to preserve the diversity encoded in early denoising stages, rather than collapsing to a small subset of modes favored by reverse-KL optimization. The motivation for supervising only the first step is discussed in Section B of the Appendix.

**Quality Supervision.** After the first step, the student model is rolled out for the remaining  $N - 1$  steps to produce a final sample  $x_\theta$ . Crucially, the output of the first step is *detached* from the computational graph before proceeding, ensuring that the gradients from the DMD loss will not propagate back into the diversity-preserving step, enforcing a clean separation of roles: the first step governs diversity, while later steps focus exclusively on quality refinement.

The overall training objective of **DP-DMD** is given by:

$$\mathcal{L} = \mathcal{L}_{\text{DMD}} + \lambda \mathcal{L}_{\text{Div}}, \quad (6)$$

where  $\lambda$  balances diversity preservation and quality refinement objectives. **Algorithm 1** presents the pseudo-code for a single training iteration.

## 5. Experiments

This section first conducts ablation studies to analyze the behavior of **DP-DMD** under different design choices, and

**Algorithm 1** DP-DMD Training for Flow-based Models

```

# x: training data batch
# k: diversity anchor step index
# t_k: anchor diffusion timestep
# N: number of student sampling steps
# lambda_div: diversity loss weight

eps = randn_like(x)
z_k = rollout_teacher(eps, k)

# diversity supervision
v_target = (eps - z_k) / (1 - t_k)
v1 = vstu(eps, 1)
loss_div = 12_loss(v1 - v_target)

# detach after first step
z1 = stopgrad(rollout_student(eps, 1))

# quality supervision
x_theta = rollout_student(z1, N - 1)
loss_dmd = dmd_loss(x_theta)

loss = loss_dmd + lambda_div * loss_div

```

then presents comprehensive comparisons and system-level evaluations to demonstrate its effectiveness in practice.

### 5.1. Experimental Setup

**Training.** We adopt the flow-based SD3.5-Medium (Esser et al., 2024) and the diffusion-based SDXL (Podell et al., 2023) as pretrained T2I backbones. All distillation experiments are conducted at an image resolution of  $1024 \times 1024$ . For the teacher model, the classifier-free guidance (CFG) scale is fixed at 3.5 for SD3.5-M and 8.0 for SDXL throughout training. Both the student and fake models are optimized using AdamW (Loshchilov & Hutter, 2017) with a learning rate of  $1 \times 10^{-5}$ . The weighting coefficient  $\lambda$  is set to  $5 \times 10^{-2}$ , the fake-model update interval  $M$  is fixed to 5, and the diversity anchor step  $K$  is also set to 5. Training is conducted on the DiffusionDB (Wang et al., 2023b) dataset using text prompts only, for a total of  $6 \times 10^3$  iterations, with a batch size of 4 per GPU across 8 NVIDIA A800 GPUs.

**Evaluation.** For evaluation, we assess sample diversity using DINOv3-ViT-Large (DINO) (Siméoni et al., 2025) and CLIP-ViT-Large (CLIP) (Radford et al., 2021) by computing the cosine similarity between extracted image feature representations in a pairwise manner:

$$\text{Diversity} = 1 - \frac{2}{L(L-1)} \sum_{i,j} \cos(\mathbf{x}_\theta^{(i)}, \mathbf{x}_\theta^{(j)}), \quad (7)$$

where  $L$  denotes the number of distinct initial noise samples per text prompt<sup>3</sup>, and we set  $L = 9$  in our experiments. In addition, we adopt VisualQuality-R1 (VQ-R1) (Wu et al., 2025) and MANIQA (MIQQA) (Yang et al., 2022) as visual

<sup>3</sup>For each text prompt, every pair of generated images is compared once, yielding  $\binom{L}{2}$  total comparisons.

**Table 1. Diversity anchor step  $K$ .** We investigate how applying diversity supervision at different teacher denoising steps influences sample diversity, visual quality, and human preference. “Base” refers to using the DMD (Yin et al., 2024a) loss without additional regularization. The best-performing results are highlighted in **bold**.

$K$	Diversity		Quality		Preference	
	DINO↑	CLIP↑	VQ-R1↑	MIQQA↑	ImgR↑	PicS↑
Base	0.137	0.133	<b>4.649</b>	1.016	<b>1.189</b>	21.75
1	0.157	0.155	4.578	0.995	1.121	21.62
3	0.175	0.178	4.648	1.016	1.125	21.67
5	0.179	0.182	4.646	<b>1.017</b>	1.142	21.76
10	<b>0.187</b>	<b>0.185</b>	4.589	1.004	1.112	<b>21.78</b>
30	<b>0.187</b>	0.181	4.602	1.007	1.117	21.71

**Table 2. Weighting coefficient  $\lambda$ .**  $\lambda$  controls the trade-off between diversity preservation and quality refinement.  $K = 3$  in all experiments.

$\lambda$	Diversity		Quality		Preference	
	DINO↑	CLIP↑	VQ-R1↑	MIQQA↑	ImgR↑	PicS↑
Base	0.137	0.133	4.649	<b>1.016</b>	<b>1.189</b>	21.75
0.01	0.170	0.164	<b>4.672</b>	1.003	1.136	<b>21.81</b>
0.05	0.175	<b>0.178</b>	4.648	<b>1.016</b>	1.125	21.67
0.08	0.176	0.176	4.662	1.014	1.117	21.71
0.10	<b>0.177</b>	0.177	4.662	1.001	1.056	21.64

quality metrics. Human preference is further evaluated using ImageReward (ImgR) (Xu et al., 2023) and PickScore (PicS) (Kirstain et al., 2023).

### 5.2. Ablation Study

We start by systematically analyzing the following properties of our methods, evaluated on the Pick-a-Pic (Kirstain et al., 2023) dataset.

**Diversity anchor step  $K$ .** We investigate the effect of the diversity anchor step  $K$  on sample diversity, visual quality, and human preference, with results summarized in Table 1. Several observations can be made. First, introducing diversity supervision at any anchor step consistently improves sample diversity compared to the baseline DMD (Yin et al., 2024b) without regularization. This demonstrates that the proposed diversity-preserving objective is effective across a wide range of denoising stages, validating the general applicability of our design. Second, we observe a clear trend that anchoring diversity supervision at later denoising steps (larger  $K$ ) leads to progressively higher diversity scores. This phenomenon aligns well with our motivation in Section 4. Third, while larger values of  $K$  yield stronger diversity gains, excessively late anchors may introduce a mild trade-off with visual quality and preference metrics. This suggests that the choice of  $K$  provides a controllable knob

Table 3. **Quantitative comparison of DMD variants** on Pick-a-Pic (Kirstain et al., 2023) and COCO-10K 2014 (Lin et al., 2014). All methods use the same backbone and inference steps (4-NFE). **DP-DMD** achieves improved diversity while maintaining competitive visual quality and human preference, without introducing perceptual or adversarial modules. Top two results are highlighted in **bold** and underline, respectively.

Method	Image-Free	NFE	Pick-a-Pic				COCO-10K 2014							
			Diversity		Quality		Preference		Diversity		Quality		Preference	
SD3.5-M-based (CFG=3.5)														
Base Model	-	60	0.240	0.221	4.657	1.020	1.007	21.80	0.288	0.204	4.636	1.043	0.910	22.31
DMD	✓	4	0.137	0.133	<b>4.649</b>	<u>1.016</u>	<b>1.189</b>	<u>21.75</u>	0.210	0.154	<b>4.690</b>	<b>1.060</b>	<b>1.053</b>	<u>22.40</u>
DMD-LPIPS	✗	4	0.169	0.169	4.598	1.005	1.063	21.62	0.204	0.168	4.599	1.012	0.949	22.29
DMD-GAN	✗	4	<b>0.183</b>	0.162	4.525	0.984	1.033	21.63	<u>0.214</u>	<u>0.174</u>	4.584	0.983	0.751	22.02
<b>DP-DMD</b>	✓	4	<u>0.179</u>	<b>0.182</b>	4.646	<b>1.017</b>	1.142	<b>21.76</b>	<b>0.250</b>	<b>0.182</b>	4.689	<u>1.032</u>	<u>0.988</u>	<b>22.41</b>
SDXL-based (CFG=8.0)														
Base Model	-	100	0.219	0.204	4.675	1.033	1.016	21.96	0.269	0.219	4.637	1.056	0.820	22.54
DMD	✓	4	0.109	0.133	<b>4.667</b>	0.971	0.951	21.68	0.139	<u>0.143</u>	4.643	0.982	0.712	22.21
DMD-LPIPS	✗	4	<u>0.136</u>	<u>0.139</u>	4.610	<u>0.976</u>	0.883	21.74	<u>0.181</u>	0.137	4.723	0.984	0.729	22.38
DMD-GAN	✗	4	0.126	0.124	<u>4.624</u>	<b>1.019</b>	<b>1.036</b>	<b>21.80</b>	0.157	0.117	<b>4.789</b>	<u>1.030</u>	<u>0.801</u>	<b>22.63</b>
<b>DP-DMD</b>	✓	4	<b>0.173</b>	<b>0.161</b>	4.591	0.954	1.011	<u>21.75</u>	<b>0.204</b>	<b>0.157</b>	4.765	<b>1.041</b>	<b>0.835</b>	<u>22.45</u>

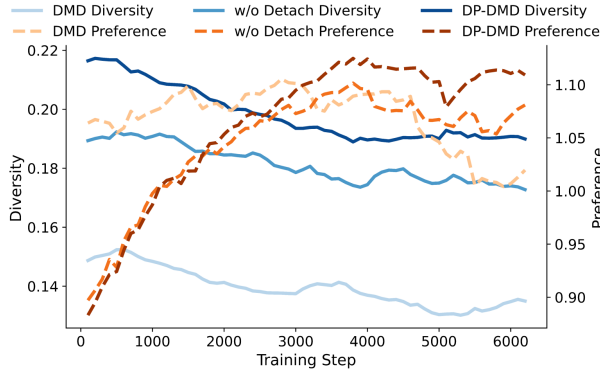


Figure 3. **Gradient stopping in DP-DMD.** Training dynamics of diversity and preference for DMD, **DP-DMD**, and a variant without gradient stopping after the first step. All curves start from the 100-th training iteration and are smoothed using exponential moving average.

to balance diversity preservation and quality refinement, and that anchoring diversity at moderately early teacher steps is most effective in practice.

**Weighting coefficient  $\lambda$ .** As shown in Table 2, increasing  $\lambda$  consistently improves sample diversity (e.g., DINO from 0.170 at  $\lambda = 0.01$  to 0.177 at  $\lambda = 0.10$ ), while slightly degrading visual quality and human preference metrics. This trade-off reflects a fundamental **generalization-memorization** balance in few-step diffusion distillation: the reverse-KL-based DMD objective encourages mode-seeking by penalizing low-density regions of the teacher distribution, causing the student to concentrate probability mass on

a small set of high-likelihood samples that can be reliably reproduced within limited steps, which manifests as partial memorization and reduced diversity. Increasing  $\lambda$  counteracts this effect by enforcing early-step diversity supervision, promoting broader mode coverage while preserving competitive visual quality at moderate values (e.g.,  $\lambda = 0.05$ ).

**Gradient stopping in DP-DMD.** Figure 3 compares **DP-DMD** with and without stopping gradients after the first step. The first point (at the 100-th iteration) already shows a sharp diversity drop when gradients are not stopped, indicating that the DMD objective starts driving mode collapse very early. As training proceeds, both variants exhibit a gradual reduction in diversity accompanied by a steady improvement in perceptual quality, reflecting the inherent generalization-memorization trade-off discussed earlier. However, the stop-gradient version consistently retains a higher level of diversity than the non-detached variant throughout training. Importantly, this improved diversity preservation does not come at the cost of perceptual quality, as their preference curves remain largely comparable. These results indicate that gradient stopping enables more persistent *diversity retention* by preventing later-step DMD optimization from progressively overriding the first-step diversity supervision, while still allowing continuous refinement of visual quality.

### 5.3. Comparison with State-of-the-Art Methods

**Comparison of Diversity Supervision.** We aim to mitigate the issue of sample diversity degradation in DMD. We compare our approach with two widely adopted baselines: incorporating a perceptual loss based on LPIPS (Zhang et al., 2018; Yin et al., 2024b) and introducing an adversar-

Half cat, Half woman, A princess, Highly detailed face, ultra-realistic, Jewelry.



Figure 4. **Qualitative comparison of diversity supervision methods.** Visual results of four distillation variants on the same prompts: (a) vanilla DMD, (b) DMD-LPIPS, (c) DMD-GAN, and (d) the proposed **DP-DMD**. While perceptual and GAN-based approaches provide limited or unstable diversity gains and often suffer quality degradation, **DP-DMD** preserves rich sample diversity while maintaining high visual fidelity, demonstrating a more favorable diversity–quality trade-off.

ial loss (Yin et al., 2024a; Chadebec et al., 2025), referred to as DMD-LPIPS and DMD-GAN, respectively. To ensure a fair comparison, all models are trained on the same dataset using an identical number of training iterations, with the same CFG scale and NFE.

Compared to prior regularization-based approaches, Table 3 shows that incorporating LPIPS as an additional constraint does not consistently yield proportional gains in diversity over vanilla DMD, while introducing extra optimization constraints that are not directly aligned with the objective of distribution matching. GAN-based regularization can also improve diversity to some extent<sup>4</sup>, but it comes with a noticeable quality/preference degradation (see Figure 4), reflecting the typical sensitivity and instability of adversarial objectives in few-step distillation. Beyond the metric trade-offs, both LPIPS and GAN variants require **extra modules** (perceptual backbone or discriminator), which increases compute/memory cost and complicates tuning.

In contrast, **DP-DMD** achieves a substantially better balance between diversity and visual quality. This improve-

ment arises from its role-separated design, which controls the diversity-quality trade-off through the anchor step  $K$  and weight  $\lambda$ . Diversity is enforced only at the first step governing global structure, allowing later steps to focus purely on quality refinement under standard DMD. Moreover, by operating entirely in latent space and introducing a stop-gradient boundary, the method avoids extra modules and prevents later-step DMD gradients from overriding early-stage diversity signals, resulting in a **lightweight** and **stable** distillation framework with more favorable trade-offs. Consistent conclusions are also observed in Section D of the Appendix through a human user study.

**System-level Comparison.** We further perform a system-level comparison by distilling our models on SD3-M (Esser et al., 2024) and benchmarking them against representative open-source few-step distillation methods. These include flow-based approaches such as Hyper-SD (Ren et al., 2024), Flash Diffusion (Chadebec et al., 2025), and TDM (Luo et al., 2025). We emphasize that this comparison is not strictly controlled, as the methods differ in training data, distillation CFG scales, optimization budgets, and other implementation details<sup>5</sup>.

<sup>4</sup>We observe that a degradation in sample quality can partially affect the **reliability** of diversity measurements, as visually evidenced in Figure 4.

<sup>5</sup>The quantitative results are presented not as a strictly fair

Table 4. **System-level comparison** of few-step open-source diffusion distillation methods. **DP-DMD** balances visual quality and diversity without perceptual or adversarial components, achieving competitive open-source performance.

Method	Image-Free	NFE	Pick-a-Pic				COCO-10K 2014							
			Diversity	Quality	Preference	Diversity	Quality	Preference	Diversity	Quality	VQ-R1↑	MIQA↑	ImgR↑	PicS↑
Base Model	-	60	0.230	0.205	4.665	1.042	1.067	21.46	0.278	0.202	4.757	1.065	1.014	22.50
Hyper-SD	×	8	<b>0.234</b>	<b>0.225</b>	4.268	0.917	0.808	20.77	<b>0.297</b>	<b>0.236</b>	3.929	0.924	0.661	21.56
Flash	×	4	0.184	0.172	4.625	<b>1.023</b>	1.014	<b>21.62</b>	0.229	0.184	4.517	0.998	0.878	<b>22.38</b>
TDM	✓	4	0.148	0.167	<b>4.675</b>	1.013	<b>1.134</b>	21.21	0.196	0.172	4.617	1.046	0.998	21.49
<b>DP-DMD</b>	✓	4	0.162	<u>0.181</u>	4.673	1.001	1.128	21.15	0.197	0.174	<b>4.672</b>	<b>1.048</b>	<b>1.034</b>	<u>22.29</u>

*Dark-haired Valerian and redhead Laureline, time and space agents, detailed and realistic painting by Carl Bloch*



Figure 5. **Qualitative comparison** with open-source few-step distillation methods.

Table 5. **Quantitative comparison on GenEval** of the model distilled using our proposed **DP-DMD** method and the original teacher model SD3.5-M.

Method	Overall	Single	Two	Count.	Colors	Pos.	Color Attr.
		Obj.	Obj.				
SD3.5-M	<b>0.66</b>	0.98	0.78	<b>0.64</b>	<b>0.83</b>	0.18	<b>0.53</b>
<b>DP-DMD</b>	0.65	<b>0.99</b>	<b>0.81</b>	0.60	0.81	<b>0.21</b>	0.48

Instead, this comparison is designed to highlight a key practical takeaway. Table 4 summarizes the system-level comparison. Without introducing any additional tricks or auxiliary modules, our approach achieves a competitive system-level trade-off. By augmenting the standard DMD (Yin et al., 2024b) objective with lightweight diversity supervision and role separation, **DP-DMD** attains comparable and sometimes stronger visual quality (see Figure 5) and sample diversity than prior DMD-based systems that rely on heavier regularization, such as perceptual backbones (Hyper-SD) or adversarial training (Flash Diffusion), validating the effectiveness and practicality of **DP-DMD**.

#### 5.4. More Results

We further evaluate our distilled model on GenEval (Ghosh et al., 2023) to verify that the proposed **DP-DMD** does not compromise core prompt-following abilities while accelerating

comparison, but to contextualize the performance of our method within the open-source ecosystem.

ating inference. GenEval evaluates compositional reasoning and instruction adherence under controlled text prompts. As shown in Table 5, **DP-DMD** achieves an overall score comparable to the teacher SD3.5-M (Esser et al., 2024), with particularly consistent performance on single/two-object composition and spatial positioning. These results suggest that our role-separated distillation preserves the teacher’s semantic alignment and compositional capabilities, while providing fast few-step sampling.

## 6. Discussion and Conclusion

We propose **DP-DMD**, a role-separated distillation framework that improves sample diversity while maintaining competitive visual quality and preference, without additional modules. Experiments across multiple T2I backbones and benchmarks show that **DP-DMD** is a lightweight and stable alternative to regularization-based approaches.

**Limitations and Future Directions.** **DP-DMD** currently provides *explicit* diversity supervision only at the first distilled step, while the subsequent steps are trained solely under the DMD objective. Although this separation is effective and easy to implement, it may be suboptimal in scenarios where diversity-relevant decisions are not fully resolved in the first step, or when later steps still influence global attributes (e.g., composition changes induced by strong guidance or challenging prompts). A natural direction is to move beyond a fixed role split and enable *step-wise* and *adaptive* balancing between diversity preservation and quality refine-

ment. We believe such adaptive, trajectory-wide supervision can further improve the balance between diversity and quality and enhance the robustness of few-step distillation across a wide range of generative settings.

## References

Chadebec, C., Tasar, O., Benaroche, E., and Aubin, B. Flash diffusion: Accelerating any conditional diffusion model for few steps image generation. In *Association for the Advancement of Artificial Intelligence*, pp. 15686–15695, 2025.

Chen, R. T., Rubanova, Y., Bettencourt, J., and Duvenaud, D. K. Neural ordinary differential equations. In *Advances in Neural Information Processing Systems*, pp. 6572–6583, 2018.

Ding, K., Ma, K., Wang, S., and Simoncelli, E. P. Image quality assessment: Unifying structure and texture similarity. *IEEE Transactions on Pattern Analysis and Machine Intelligence*, 44(5):2567–2581, 2020.

Esser, P., Kulal, S., Blattmann, A., Entezari, R., Müller, J., Saini, H., Levi, Y., Lorenz, D., Sauer, A., Boesel, F., et al. Scaling rectified flow Transformers for high-resolution image synthesis. In *International Conference on Machine Learning*, 2024.

Geng, Z., Deng, M., Bai, X., Kolter, J. Z., and He, K. Mean flows for one-step generative modeling. *arXiv preprint arXiv:2505.13447*, 2025.

Ghosh, D., Hajishirzi, H., and Schmidt, L. GENEVAL: An object-focused framework for evaluating text-to-image alignment. In *Advances in Neural Information Processing Systems*, pp. 52132–52152, 2023.

He, X., Fu, S., Zhao, Y., Li, W., Yang, J., Yin, D., Rao, F., and Zhang, B. TempFlow-GRPO: When timing matters for GRPO in flow models. *arXiv preprint arXiv:2508.04324*, 2025.

Kirstain, Y., Polyak, A., Singer, U., Matiana, S., Penna, J., and Levy, O. Pick-a-Pic: An open dataset of user preferences for text-to-image generation. In *Advances in Neural Information Processing Systems*, pp. 36652–36663, 2023.

Labs, B. F., Batifol, S., Blattmann, A., Boesel, F., Consul, S., Diagne, C., Dockhorn, T., English, J., English, Z., Esser, P., et al. FLUX. 1 Kontext: Flow Matching for in-context image generation and editing in latent space. *arXiv preprint arXiv:2506.15742*, 2025.

Li, R., Yang, T., Guo, S., and Zhang, L. RORem: Training a robust object remover with human-in-the-loop. In *IEEE/CVF Conference on Computer Vision and Pattern Recognition*, pp. 14024–14035, 2025.

Lin, S., Wang, A., and Yang, X. SDXL-Lightning: Progressive adversarial diffusion distillation. *arXiv preprint arXiv:2402.13929*, 2024.

Lin, T.-Y., Maire, M., Belongie, S., Hays, J., Perona, P., Ramanan, D., Dollár, P., and Zitnick, C. L. Microsoft COCO: Common objects in context. In *European Conference on Computer Vision*, pp. 740–755, 2014.

Lipman, Y., Chen, R. T., Ben-Hamu, H., Nickel, M., and Le, M. Flow Matching for generative modeling. In *International Conference on Machine Learning*, 2022.

Liu, D., Gao, P., Liu, D., Du, R., Li, Z., Wu, Q., Jin, X., Cao, S., Zhang, S., Li, H., et al. Decoupled DMD: CFG augmentation as the spear, distribution matching as the shield. *arXiv preprint arXiv:2511.22677*, 2025.

Liu, E., Ning, X., Lin, Z., Yang, H., and Wang, Y. OMS-DPM: Optimizing the model schedule for diffusion probabilistic models. In *International Conference on Machine Learning*, 2023a.

Liu, X., Gong, C., and Liu, Q. Flow straight and fast: Learning to generate and transfer data with rectified flow. In *International Conference on Learning Representations*, 2023b.

Liu, X., Zhang, X., Ma, J., Peng, J., et al. InstaFlow: One step is enough for high-quality diffusion-based text-to-image generation. In *International Conference on Learning Representations*, 2023c.

Loshchilov, I. and Hutter, F. Decoupled weight decay regularization. In *International Conference on Learning Representations*, 2017.

Lu, C. and Song, Y. Simplifying, stabilizing and scaling continuous-time consistency models. *arXiv preprint arXiv:2410.11081*, 2024.

Lu, Y., Ren, Y., Xia, X., Lin, S., Wang, X., Xiao, X., Ma, A. J., Xie, X., and Lai, J.-H. Adversarial distribution matching for diffusion distillation towards efficient image and video synthesis. In *IEEE/CVF International Conference on Computer Vision*, pp. 16818–16829, 2025.

Luo, S., Tan, Y., Patil, S., Gu, D., Von Platen, P., Passos, A., Huang, L., Li, J., and Zhao, H. LCM-LoRA: A universal stable-diffusion acceleration module. *arXiv preprint arXiv:2311.05556*, 2023.

Luo, Y., Hu, T., Sun, J., Cai, Y., and Tang, J. Learning few-step diffusion models by trajectory distribution matching. *arXiv preprint arXiv:2503.06674*, 2025.

Meng, C., Rombach, R., Gao, R., Kingma, D., Ermon, S., Ho, J., and Salimans, T. On distillation of guided diffusion models. In *IEEE/CVF Conference on Computer Vision and Pattern Recognition*, pp. 14297–14306, 2023.

Podell, D., English, Z., Lacey, K., Blattmann, A., Dockhorn, T., Müller, J., Penna, J., and Rombach, R. Sdxl: Improving latent diffusion models for high-resolution image synthesis. *arXiv preprint arXiv:2307.01952*, 2023.

Poole, B., Jain, A., Barron, J. T., and Mildenhall, B. DreamFusion: Text-to-3d using 2d diffusion. *arXiv preprint arXiv:2209.14988*, 2022.

Poole, B., Jain, A., Barron, J. T., and Mildenhall, B. DreamFusion: Text-to-3d using 2d diffusion. In *International Conference on Learning Representations*, 2023.

Radford, A., Kim, J. W., Hallacy, C., Ramesh, A., Goh, G., Agarwal, S., Sastry, G., Askell, A., Mishkin, P., Clark, J., et al. Learning transferable visual models from natural language supervision. In *International Conference on Machine Learning*, 2021.

Ren, Y., Xia, X., Lu, Y., Zhang, J., Wu, J., Xie, P., Wang, X., and Xiao, X. Hyper-SD: Trajectory segmented consistency model for efficient image synthesis. In *Advances in Neural Information Processing Systems*, pp. 117340–117362, 2024.

Rombach, R., Blattmann, A., Lorenz, D., Esser, P., and Ommer, B. High-resolution image synthesis with latent diffusion models. In *IEEE/CVF Conference on Computer Vision and Pattern Recognition*, pp. 10684–10695, 2022.

Sauer, A., Boesel, F., Dockhorn, T., Blattmann, A., Esser, P., and Rombach, R. Fast high-resolution image synthesis with latent adversarial diffusion distillation. In *ACM SIGGRAPH Conference*, pp. 1–11, 2024a.

Sauer, A., Lorenz, D., Blattmann, A., and Rombach, R. Adversarial diffusion distillation. In *European Conference on Computer Vision*, pp. 87–103, 2024b.

Siméoni, O., Vo, H. V., Seitzer, M., Baldassarre, F., Oquab, M., Jose, C., Khalidov, V., Szafraniec, M., Yi, S., Ramamonjisoa, M., et al. DINOv3. *arXiv preprint arXiv:2508.10104*, 2025.

Song, Y. and Dhariwal, P. Improved techniques for training consistency models. In *International Conference on Learning Representations*, 2023.

Song, Y., Sohl-Dickstein, J., Kingma, D. P., Kumar, A., Ermon, S., and Poole, B. Score-based generative modeling through stochastic differential equations. In *International Conference on Learning Representations*, 2020.

Song, Y., Dhariwal, P., Chen, M., and Sutskever, I. Consistency models. In *International Conference on Machine Learning*, 2023.

Sutton, R. S., Barto, A. G., et al. Reinforcement learning. *Journal of Cognitive Neuroscience*, 11(1):126–134, 1999.

Tong, S., Ma, N., Xie, S., and Jaakkola, T. Flow map distillation without data. *arXiv preprint arXiv:2511.19428*, 2025.

Wan, T., Wang, A., Ai, B., Wen, B., Mao, C., Xie, C.-W., Chen, D., Yu, F., Zhao, H., Yang, J., et al. WAN: Open and advanced large-scale video generative models. *arXiv preprint arXiv:2503.20314*, 2025.

Wang, B. and Vastola, J. J. Diffusion models generate images like painters: an analytical theory of outline first, details later. *arXiv preprint arXiv:2303.02490*, 2023.

Wang, F.-Y., Huang, Z., Bergman, A., Shen, D., Gao, P., Lingelbach, M., Sun, K., Bian, W., Song, G., Liu, Y., et al. Phased consistency models. In *Advances in Neural Information Processing Systems*, pp. 83951–84009, 2024.

Wang, Z., Lu, C., Wang, Y., Bao, F., Li, C., Su, H., and Zhu, J. ProlificDreamer: High-fidelity and diverse text-to-3d generation with variational score distillation. In *Advances in Neural Information Processing Systems*, pp. 8406–8441, 2023a.

Wang, Z. J., Montoya, E., Munechika, D., Yang, H., Hoover, B., and Chau, D. H. DiffusionDB: A large-scale prompt gallery dataset for text-to-image generative models. In *Association for Computational Linguistics*, pp. 893–911, 2023b.

Wu, T., Zou, J., Liang, J., Zhang, L., and Ma, K. VisualQuality-R1: Reasoning-induced image quality assessment via reinforcement learning to rank. *arXiv preprint arXiv:2505.14460*, 2025.

Xu, J., Liu, X., Wu, Y., Tong, Y., Li, Q., Ding, M., Tang, J., and Dong, Y. ImageReward: Learning and evaluating human preferences for text-to-image generation. In *Advances in Neural Information Processing Systems*, pp. 15903–15935, 2023.

Yan, H., Liu, X., Pan, J., Liew, J. H., Liu, Q., and Feng, J. PeRFlow: Piecewise rectified flow as universal plug-and-play accelerator. In *Advances in Neural Information Processing Systems*, pp. 78630–78652, 2024.

Yang, S., Wu, T., Shi, S., Lao, S., Gong, Y., Cao, M., Wang, J., and Yang, Y. MANIQA: Multi-dimension attention network for no-reference image quality assessment. In *IEEE/CVF Conference on Computer Vision and Pattern Recognition Workshops*, pp. 1191–1200, 2022.

Yin, T., Gharbi, M., Park, T., Zhang, R., Shechtman, E., Durand, F., and Freeman, B. Improved distribution matching distillation for fast image synthesis. In *Advances in Neural Information Processing Systems*, pp. 47455–47487, 2024a.

Yin, T., Gharbi, M., Zhang, R., Shechtman, E., Durand, F., Freeman, W. T., and Park, T. One-step diffusion with distribution matching distillation. In *IEEE/CVF Conference on Computer Vision and Pattern Recognition*, pp. 6613–6623, 2024b.

Zhang, R., Isola, P., Efros, A. A., Shechtman, E., and Wang, O. The unreasonable effectiveness of deep features as a perceptual metric. In *IEEE/CVF Conference on Computer Vision and Pattern Recognition*, pp. 586–595, 2018.

Zheng, K., Wang, Y., Ma, Q., Chen, H., Zhang, J., Balaji, Y., Chen, J., Liu, M.-Y., Zhu, J., and Zhang, Q. Large scale diffusion distillation via score-regularized continuous-time consistency. *arXiv preprint arXiv:2510.08431*, 2025.

Zhou, M., Zheng, H., Gu, Y., Wang, Z., and Huang, H. Adversarial score identity distillation: Rapidly surpassing the teacher in one step. *arXiv preprint arXiv:2410.14919*, 2024a.

Zhou, M., Zheng, H., Wang, Z., Yin, M., and Huang, H. Score identity distillation: Exponentially fast distillation of pretrained diffusion models for one-step generation. In *International Conference on Machine Learning*, 2024b.

## Appendix

### A. Observation of Early and Late Denoising Steps

Figure A visualizes the inference process of SD3.5-M (Esser et al., 2024) under different noise initializations.

As shown in the left panel of Figure A, the denoising trajectory exhibits a clear stage-wise behavior. The early denoising steps, operating at high noise levels, primarily determine the global structural layout of the generated image, including object identity, coarse geometry, and overall composition. Notably, variations introduced at these early stages persist throughout the remainder of the denoising process, resulting in distinct final samples even under identical text conditioning. This observation highlights a strong connection between early denoising behavior and **sample diversity**.

The right panel of Figure A further illustrates this phenomenon by comparing early denoising steps across different noise initializations. Even at very early timesteps, noticeable differences in global structure already emerge, indicating that diversity is largely established before fine details are formed.

In contrast, later denoising steps operate at lower noise levels and mainly focus on refining fine-grained visual details such as textures, colors, and local appearance. These steps exhibit limited influence on the global structure and contribute predominantly to perceptual quality rather than diversity.

Together, these observations suggest an intrinsic asymmetry between early and late denoising stages: early steps govern global structure and diversity, while later steps specialize in quality refinement. This motivates our design choice in **DP-DMD** to explicitly separate the training objectives of early and late distilled steps, enabling effective diversity preservation without sacrificing visual fidelity.

### B. Motivation for First-Step Diversity Supervision

A key design choice in **DP-DMD** is to apply explicit supervision only to the *first* distilled step. This choice is motivated by the alignment of state distributions between the teacher and the student during training. Specifically, both the teacher and the student are trained on the same noise prior, and therefore share the identical initial state  $\epsilon$ . As a result, the student’s first-step input lies on a distribution that has been fully observed by the teacher, making it well-defined and meaningful to construct a teacher-derived supervision signal at this step.

In contrast, the intermediate states encountered by the student during its subsequent inference steps are generated by the student itself and generally do not lie on the teacher’s training trajectory. These states are *out-of-distribution* for the teacher and thus lack reliable ground-truth targets. Applying direct supervision at later steps would therefore introduce a distribution mismatch between the teacher and student, potentially leading to biased or unstable training (Tong et al., 2025). Consequently, we restrict explicit diversity supervision to the first step, where the teacher’s guidance is both valid and informative at this stage.

### C. DP-DMD on Diffusion Models

Early diffusion models such as SDXL (Podell et al., 2023) differ from flow-based formulations (Esser et al., 2024) in that they are typically parameterized to predict the noise  $\epsilon$  (or related quantities) rather than the velocity field  $v$ . To adapt our diversity supervision to this setting, we formulate the supervision directly in the  $x_0$  (denoised latent) space, which is naturally available under common schedulers (e.g., DDIM).

Concretely, given an intermediate teacher latent  $z_{t_k}$  at timestep  $t_k$ , we compute the teacher-implied denoised prediction as:

$$z_k^{\text{target}} = \frac{z_{t_k} - \sqrt{1 - \alpha_{t_k}} \epsilon_{\text{tea}}(z_{t_k}, t_k)}{\sqrt{\alpha_{t_k}}} \quad (8)$$

where  $\epsilon_{\text{tea}}(z_{t_k}, t_k)$  is the noise prediction produced by the frozen teacher model. The resulting  $z_k^{\text{target}}$  serves as the diffusion-model counterpart of the teacher-derived intermediate supervision used in the flow-based case.

For the distilled student model, we compute its first-step prediction  $z_\theta(z_T, T)$  from the initial noisy latent  $z_T$  at the starting timestep  $T$ . We then encourage the student’s first step to match the teacher-derived target via an  $\ell_2$  regression loss:

$$\mathcal{L}_{\text{Div}} = \mathbb{E}_{z_T} \left[ \|z_\theta(z_T, T) - z_k^{\text{target}}\|^2 \right]. \quad (9)$$

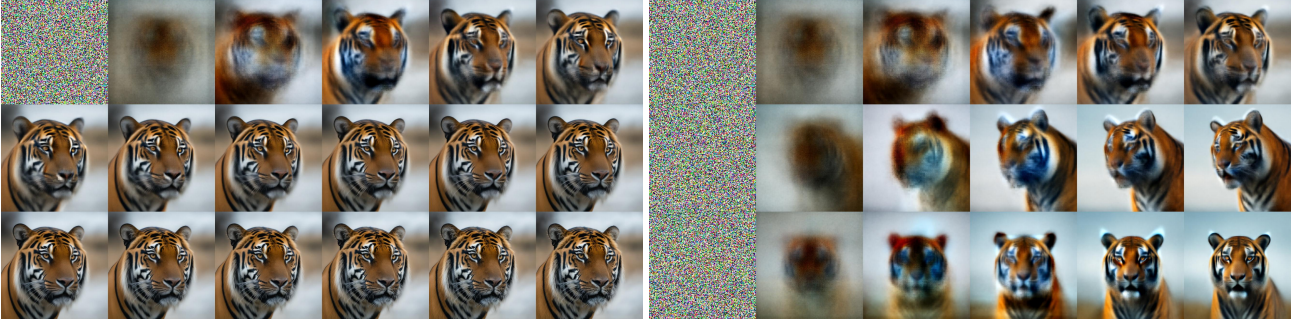


Figure A. **Progressive denoising dynamics.** Visualization of SD3.5-M (Esser et al., 2024) inference exhibits a stage-wise denoising pattern. The left panel shows a trajectory from step 1 to step 17, while the right panel highlights early steps under different noise initializations. Early steps recover the global structural layout, already showing variation across samples and suggesting a strong link to sample **diversity**, whereas later steps refine fine-grained appearance details and textures.

---

**Algorithm 2 DP-DMD** Training for Diffusion Models

```

# x: training data batch
# k: diversity anchor step index
# T: starting timestep
# N: number of student sampling steps
# lambda_div: diversity loss weight

eps = randn_like(x)
z_k, eps_z0_tea, a_k = rollout.teacher.target(eps, k, T)

# convert to x0 for diversity supervision
z0_target = (z_k - sqrt(1 - a_k) * eps_z0_tea) / sqrt(a_k)

# diversity supervision
eps_z0_stu, a_T = eps_stu(eps, T)
z0_stu = (eps - sqrt(1 - a_T) * eps_z0_stu) / sqrt(a_T)
loss_div = l2_loss(z0_stu - z0_target)

# detach after first step
z_T_minus_1 = stopgrad(rollout.student(eps, 1))

# quality supervision
z0_theta = rollout.student(z_T_minus_1, N - 1)
loss_dmd = dmd_loss(z0_theta)

loss = loss_dmd + lambda_div * loss_div

```

---

This diversity supervision mirrors our flow-based objective in spirit: it anchors the student’s early denoising behavior to a teacher-defined intermediate target, thereby promoting broader mode coverage and mitigating diversity degradation in few-step diffusion distillation. The overall pseudo-code for applying **DP-DMD** to diffusion-based models (*e.g.*, SDXL) is shown in [Algorithm 2](#).

## D. User Study

We conduct a controlled user study to evaluate both **sample diversity** and **image quality** of different distillation methods. We randomly select 50 text prompts and recruit 10 participants with prior experience in evaluating image generation results. For each prompt, images generated by two methods under identical text conditioning and random seed settings are presented side by side in randomized order.

Participants are asked to perform pairwise comparisons along two criteria: (1) Diversity, focusing on variations in global structure, composition, and semantic attributes across multiple samples generated from the same prompt; and (2) Image quality, reflecting visual fidelity, realism, and overall perceptual quality of the generated images. No additional guidance is provided beyond these criteria to avoid bias.

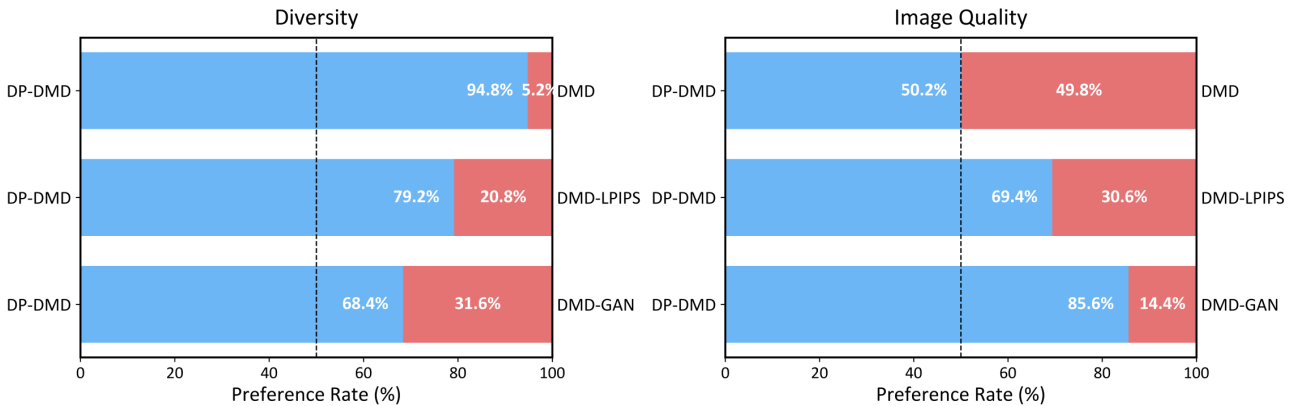


Figure B. **User study on diversity and image quality.** We run pairwise comparisons on 50 prompts with 10 participants for (left) diversity and (right) image quality. Bars show win rates (%) of **DP-DMD** against DMD (Yin et al., 2024a), DMD-LPIPS, and DMD-GAN; the dashed line marks 50%. **DP-DMD** is consistently preferred, achieving higher diversity while maintaining strong image quality.

The final results are reported as win rates aggregated over all prompts and users. As shown in Figure B, **DP-DMD** is consistently preferred over DMD (Yin et al., 2024a), DMD-LPIPS, and DMD-GAN, showing substantial improvements in diversity while maintaining competitive or superior image quality. These results indicate that the proposed role-separated distillation effectively mitigates *mode collapse* without sacrificing perceptual quality.

## E. More Visualizations

We provide additional qualitative results in Figure C and Figure D to complement the quantitative analysis in the main paper. Figure C focuses on sample diversity under identical text prompts and different random seeds. The results show that **DP-DMD** consistently produces a wider range of global structures, compositions, and semantic variations, effectively mitigating the mode collapse behavior commonly observed in vanilla DMD (Yin et al., 2024b;a).

In contrast, Figure D exclusively presents samples generated by **DP-DMD** to demonstrate its intrinsic visual quality. Despite operating under few-step inference, the generated images exhibit realistic appearance, coherent global layouts, and fine-grained details with natural textures and colors. These results indicate that the diversity-preserving supervision in **DP-DMD** enables the model to maintain high visual quality while achieving improved sample diversity.

*A man with sunglasses.*



*A living room has a couch, a chair, and a fireplace.*



*A very cute dog wearing some type of silly hat.*



*A picture of a cute anime girl.*



(a) DMD

(b) DMD-LPIPS

(c) DMD-GAN

(d) DP-DMD

**Figure C. Sample diversity under identical prompts.** Comparison of images generated with the same text prompts and different random seeds, showing that **DP-DMD** produces more diverse global structures and semantic variations than baseline methods. All models generate samples with 4 NFEs.



**Figure D. Sample quality of DP-DMD.** Images generated at  $1024 \times 1024$  resolution by **DP-DMD**, distilled from SD3.5-M (Esser et al., 2024). All samples are produced with 4 NFEs, demonstrating high visual fidelity and coherent global structures under few-step inference.